Surface & Coatings Technology 313 (2017) 47–54

Contents lists available at ScienceDirect

Surface & Coatings Technology

journal homepage: www.elsevier.com/locate/surfcoat

Plasma nitriding of 316L stainless steel in two different N_2-H_2 atmospheres - Influence on microstructure and corrosion resistance

Evangelina De Las Heras [a], Gabriel Ybarra [b], Diego Lamas [c,d], Amado Cabo [e], Eugenia Laura Dalibon [f,*], Sonia P. Brühl [f]

[a] División Hidrógeno en Materiales, Gerencia Materiales, GAEN, Centro Atómico Constituyentes, Av. Gral. Paz 1499, San Martín B1650KNA, Buenos Aires, Argentina
[b] Research Center on Surface Processes, Nanomaterials Unit, National Institute of Industrial Technology (INTI), C.C.157, San Martín B1650KNA, Buenos Aires, Argentina
[c] CONICET, Argentina
[d] Escuela de Ciencia y Tecnología, Universidad Nacional de General San Martín, Martín de Irigoyen 3100, Edificio Tornavía, Campus Miguelete, 1650 San Martín, Buenos Aires, Argentina
[e] IONAR S.A., Arias 3422, C1430CRB, Buenos Aires, Argentina
[f] Surface Engineering Group, Universidad Tecnológica Nacional (UTN-FRCU), Ing. Pereira 676, E3264BTD Concepción del Uruguay, Argentina

ARTICLE INFO

Article history:
Received 8 August 2016
Revised 9 January 2017
Accepted in revised form 10 January 2017
Available online 11 January 2017

Keywords:
AISI 316L
Ion nitriding
Corrosion resistance

ABSTRACT

Plasma nitriding of austenitic stainless steel is of high technological importance due to its ability to improve the surface hardness, wear and corrosion resistance. Therefore, such process presents a significant potential as a treatment of materials for biomedical applications. The resulting properties obtained on the nitrided layer depend on the nitriding parameters used, such as temperature, gases partial pressures, process time, among others. In this work, austenitic stainless steel AISI 316L was nitrided in a DC plasma using two different N_2-H_2 atmospheres: 25% N_2 and 20% N_2. A detailed analysis of surface microstructure has been carried out and related to corrosion behaviour in two saline solutions. The results were compared with the 316L unnitrided (UN). The chemical composition of the nitrided layer was determined by GDOES. The phases present in the nitrided layer were analysed by X-ray diffraction (XRD) and the phases in the surface of nitrided layer were analysed by grazing incidence X-ray diffraction mode (GIXRD). The corrosion behaviour of the samples was studied by an electrochemical corrosion test in 3 wt% NaCl and Ringer's solutions. The GDOES (Glow Discharge Optical Emission Spectroscopy) analysis shows a higher N concentration of in the surface of 25% N_2 samples, named HN. The phases observed, by GIXRD, in HN samples were expanded austenite γ_N, CrN, Fe_3N and Fe_4N and, in the 20% N_2 samples, named LN, only peaks of expanded austenite and Fe_4N were observed. The corrosion results showed that LN present better corrosion resistance than HN, this could be due to the absence of chromium nitrides in the surface of LN as a consequence of lower N percentage in the nitriding atmosphere.

1. Introduction

Low temperature ion nitriding (300–420 °C) is a widely used surface treatment applied on stainless steels [1], since it provides high surface hardness and wear resistance without significantly affecting its corrosion resistance [2]. At these temperatures, the Cr diffusion rate into steel is low and consequently, the formation of Cr nitrides is inhibited [3,4]. By performing a sputtering pre-treatment within the same reactor, it is possible to remove the Cr_2O_3 passivation layer, promoting the diffusion of nitrogen into the material [5]. When austenitic stainless steels are nitrided at the aforementioned temperatures, a new diffusion layer is generated and is commonly known as "expanded austenite" "γ_N" or also "S phase". This S phase is metastable and presents an fcc structure with a high nitrogen content [6–8] in solution, located in octahedral sites [9,10]. In some cases, depending on the nitriding temperature, the γ_N phase is accompanied by certain cubic (γ'-Fe_4N) and hexagonal phases (ε-$Fe_{2-3}N$) [4]. If the temperature exceeds 420 °C (693 K), the maximal solubility of nitrogen in the austenite phase is reached and the metastable phase (γ_N) is decomposed, thus generating precipitation of CrN [11–13]. The precipitation of CrN results in the depletion of free Cr from the austenitic matrix, which results in a lower corrosion resistance of the nitrided layer. Also, the nitrided layer structure depends on the nitriding parameters, such as temperature, processing time, gases partial pressures, base material superficial pre-treatment and the characteristics of the electrical discharge which generates and sustains the plasma [14–16]. In DC pulsed nitriding of austenitic stainless steels, it was observed that the processing time (t) and temperature (T) are more important than time on/off ($t_{on/off}$) and gas pressure in the treatment atmosphere. It was also confirmed that the temperature has

* Corresponding author.
E-mail addresses: lasheras@cnea.gov.ar (E. De Las Heras), gabriel@inti.gov.ar (G. Ybarra), diego_german_lamas@yahoo.com.ar (D. Lamas), cabo@ionar.com.ar (A. Cabo), dalibone@frcu.utn.edu.ar (E.L. Dalibon), sonia@frcu.utn.edu.ar (S.P. Brühl).

http://dx.doi.org/10.1016/j.surfcoat.2017.01.037
0257-8972/

greater influence on thickness, hardness and microstructure [16] of the nitrided layer than the change in pulse frequency ($t_{on/off}$) [17].

Although austenitic stainless steels are widely used in the biomaterials field, particularly in orthopaedics (in fracture fixation devices and in partial or total replacement of joints) and surgical tools [18,19], there are few studies about the in-vivo behaviour of the γ_N phase. Some of them show that the tests performed in Ringer and Hank solutions indicate that the γ_N phase shows a combination of good wear resistance and pitting corrosion [20] and excellent antibacterial property [21–23].

The aim of this study was to evaluate the change in surface structure when nitrogen content was lowered from 25% (the usual one) to 20%. Temperature was set on 400 °C and processing time was not varied from usual parameters in order to obtain a wide nitrided layer, hard and wear resistant but also corrosion resistant. The study by X-ray diffraction at small angles is directed to determine surface structure changes with the processing atmosphere. There are not many studies about the structure variation of the nitrided layers, using glancing angle XRD, and especially about the variation in the nitrogen partial pressure below 25%.

It is important to note that the plasma-assisted nitriding treatments were performed in industrial reactors, which facilitates the direct transfer of results to the industry. The potential application of this surface modification treatment in the field of biomaterials was also evaluated by performing corrosion tests in Ringer's solution.

2. Materials and methods

A typical austenitic stainless steel grade AISI 316L was utilized for the present study. The chemical composition was determined and corresponded to AISI 316L steel according to ASTM A276. Cylindrical samples of 25.4 mm in diameter and 10 mm in thickness were obtained from an as-annealed commercial bar. The microstructure was revealed by etching with a Marble reagent (10 g $CuSO_4$, 50 ml HCl, 50 ml H_2O) and the evaluation was performed using optical microscopy (OM) on a Zeiss™ Axiotech microscope, and scanning electron microscopy (SEM) on a Philips™ SEM 505. The substrate presented a microhardness of about (170 ± 10) HV_{25g}. All samples were ground with SiC abrasive papers (240, 320, 400 and 600) prior to nitriding.

Samples were treated in an ion nitriding industrial reactor (Ionar S. A., Argentina) described elsewhere [24], with other industrial components in a conventional process. Before the ion nitriding process, samples sputter cleaned in the plasma reactor with a gas mixture composed of 50/50 Ar/H_2 for 3 h so as to remove the native passive film, characteristic of stainless steels. This mixture combines the mechanical removal properties of Ar^+ and the reducing chemical effect of hydrogen on Cr_2O_3 [25]. The main experimental parameters of the two ion nitriding processes (HN and LN) are summarized in Table 1. The temperature was determined and controlled by an electrically isolated thermocouple attached to the sample holder.

Only the hydrogen/nitrogen proportion in the gas mixture was different between the two groups: HN samples were nitrided with 25% nitrogen and LN samples with only 20% nitrogen. About 15 samples were treated for each group. After the nitriding process, the samples were slowly cooled down to room temperature in a nitrogen atmosphere.

Cross-sections were prepared in order to determine the nitrided layer thickness and characteristics and to perform microhardness depth profiles, perpendicular to the surface. The chemical composition of the nitrided layer was determined on a Jobin Yvon RF GD Profiler (GDOES) equipped with an anode diameter of 4 mm and operated under an RF discharge pressure of 650 Pa and a 40 W power. Surface microhardness and depth profile measurements were made using a Vickers microindenter (Shimadzu HV-2). The experimental loads were 50 and 25 g, respectively.

The phases present in the unnitrided samples (UN) as well as in the treated ones (HN and LN), were analysed by X-ray diffraction (XRD) with a Philips PW 3710 X-ray diffractometer. A conventional θ–2θ Bragg–Brentano symmetric configuration was used, with a Bragg angle scanning ranging from 20° to 120°. The selected step size was 0.02° and the time per step was settled at 3 s. The radiation source was from a copper tube with a wavelength of $\lambda CuK\alpha = 0.15418$ nm.

As corrosion behaviour is related to close surface composition, the samples were further investigated using the grazing incidence X-ray diffraction mode (GIXRD) with incidence angles fixed at 1°, 2.5°, 5°, 15° and 22° (Table 2). The penetration depth of the X-rays was estimated within the region of the (111) peak (which is the most intense in the pattern), assuming a location of $2\theta = 43°$. GIXRD was performed on the same equipment using CuKα radiation at 40 kV and 30 mA. A "Thin Film attachment" Philips flat graphite monochromator was used, with a divergence slit of 1/12°. In all cases the sample was in the same position.

In the grazing incidence configuration, the X-rays penetration depth could be estimated using the following equation [26]:

$$d = \left[\mu\left(\frac{1}{\sin(\alpha)} + \frac{1}{\sin(2\theta-\alpha)}\right)\right]^{-1} \quad (1)$$

where α is the angle of incidence and μ is the linear absorption coefficient.

To calculate the linear absorption coefficient, μ, the mass absorption coefficient (μ/ρ, that depends only on the composition) should be multiplied by the material density, ρ. Mass absorption coefficients were obtained from the literature [26] and the depth of analysis was considered as the depth into the material measured along the surface normal where the intensity of X-rays falls to 1/e of its value at the surface. The chemical composition of the nitrided layer (obtained by GDOES) and the substrate were used to approximate the value of μ/ρ for the treated surface and the substrate. By assuming a substrate density of 8 g/cm^3, the resulting linear absorption coefficient resulted 2112 cm^{-1}. In the case of the surface, since the density is not accurately known, a first estimation gave a value of 1816 cm^{-1}. Thus, the obtained approximate values were: $(\mu/\rho)_{surface} = 227\ cm^2/g$; $(\mu/\rho)_{substrate} = 264\ cm^2/g$. Under these assumptions, the depths were obtained for the different angles of incidence used in this study.

The corrosion behaviour of the samples UN, HN and LN was studied by electrochemical corrosion tests. Several samples of each group were grounded with emery paper (1000 grit) after nitriding to clean the surface prior to corrosion tests. Potentiodynamic curves were recorded with an EG&G PAR 273A potentiostat using a three-electrode electrochemical cell with a Ag|AgCl|KCl (saturated) as reference electrode and a platinum wire as counter electrode. Only a circular area of 1 cm in diameter of the samples was exposed to the test solution, sealed

Table 1
Main parameters of the nitriding process for the two studied conditions.

Experimental parameter	Fixed conditions for LN and HN samples
Time	20 h
Temperature	400 °C
Pressure	6.5 hPa
Voltage between electrodes	700 V
Pulse discharge t_{on}–t_{off}	70–200 μs
Current density	~1 $mA \cdot cm^{-2}$

Table 2
Angular positions of experimental UN, HN and LN peaks.

Reflections	2θ experimental UN	2θ experimental HN	2θ experimental LN
111	45.53°	40.87°	40.31°
200	50.61°	45.37°	45.94°
220	74.57°	67.88°	67.65°
311	90.49°	81.35°	81.57°
222	95.89°	87.98°	87.10°

and delimitated with an O-ring [27]. One group of tests was performed in a 3% NaCl solution at room temperature, using a potential scan rate of 1 mV/s. For corrosion tests simulating body fluid, a Ringer's solution was selected for the second group of tests. The chemical composition of the solution (in g/l) was: NaCl 9.0, $CaCl_2$ 0.24, KCl 0.43, $NaHCO_3$ 0.2 (pH: 7.8 at room temperature). The selected scan rate was also 1 mV/s. Three tests were carried out in 3% NaCl solution and other two tests in Ringer's solution for each group, HN, LN and UN. Curves which are representative of each group were plotted.

3. Results

SEM micrographs (Fig. 1a and b) show that the nitrided layer is formed by an outer and an inner layer. The nitrided layers of HN and LN are composed of two layers; in the case of HN, the uppermost is about 15 μm and the bottom one, ~4 μm. In the case of LN, the uppermost is ~14 μm and the bottom one, ~2.5 μm thick.

Fig. 2, obtained through GDOES, shows nitrogen and carbon concentration depth profiles acquired in HN and LN samples, respectively. HN shows a higher concentration of nitrogen and the total nitrided layer is about 20 μm thick; whereas LN has lower nitrogen content, a larger gradient and the total nitrided layer extends to approximately 15 μm. The variation in nitrogen composition might correspond to the outer layer observed in the SEM micrographs (Fig. 1). Both nitrogen depth profiles show plateau-type shapes, slowly decreasing from the surface, followed by a rather sharp decrease, as other authors have already reported [28].

The C profiles for both samples show some small segregation of carbon at the end of the nitrided layer [29], a feature also observed by other authors [30] in nitrocarburizing processes [31]. That would be the inner layer, with not so well defined interface with the base material.

The surface hardness after the nitriding treatments in HN and LN samples, increased from 170 $HV_{0.05}$ in the initial state to 1125 ± 70 $HV_{0.05}$ and 1090 ± 50 $HV_{0.05}$, respectively. Microhardness profiles (Fig. 3) from the surface to the base material shows a transition correlated with the N composition profiles of Fig. 2.

The diffractograms of UN and HN samples are shown in Fig. 4a. The patterns corresponding to HN present the peaks corresponding to the expanded austenite, γ_N, and small amounts of iron $F_{2,3}N$ and Fe_4N and chromium nitrides (CrN). Table 2 presents the 2θ positions of the observed peaks.

From the analysis of the Fig. 4 and Table 2, it is noted that the experimental peaks of expanded austenite, γ_N, for HN and LN, are broadened and also shifted to lower angles 2θ with respect to the substrate austenite UN. With the position of the experimental peak (111) and Bragg's law, a lattice expansion in 12% average for both nitrided samples was calculated. The shift effect of the peaks could indicate the presence of compressive residual stresses [17] and/or stacking faults that can occur in fcc structures [32].

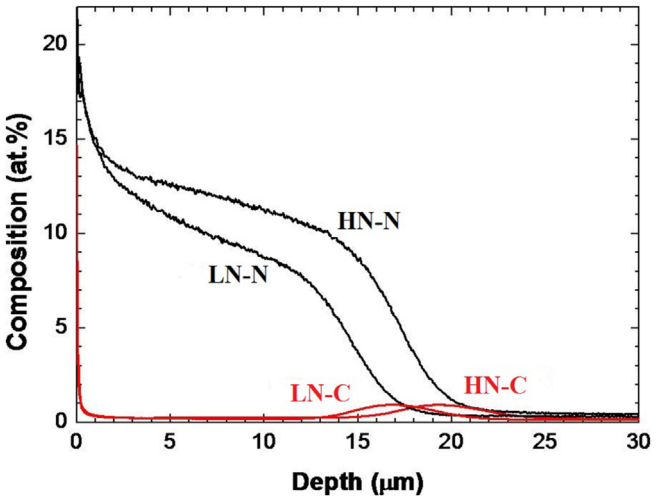

Fig. 2. GDOES element (C and N) concentration depth profile acquired from HN and LN.

Table 3 presents reflections that were unambiguously identified with different nitrides, for example, peaks in 2θ = 63.62° with CrN in HN, 57.8° with $Fe_{2,3}N$ in HN, 33.7° and 70.2° with Fe_4N in LN.

3.1. Grazing incidence X-ray diffraction

X-ray penetration at 2θ = 30° and 55° are shown in Table 4. Since the penetration for 10° and higher angles is practically equal to the penetration at normal incidence in the Bragg Brentano geometry, and the patterns obtained for 2.5° were very similar to those for 1°, those XRD patterns will not be presented here. Therefore, only the patterns obtained at 1° and 5° for HN and LN samples will be referred in following discussions.

X-ray spectra at 1° for HN and LN are shown in Fig. 5a. In the case of HN, the peaks corresponding to CrN, Fe_3N and Fe_4N and expanded austenite are clearly noticed. Furthermore, there is evidence of αFe (110) that occurs when the expanded austenite phase shifts from a metastable phase into two stable phases (αFe and Cr nitrides), when the temperature and the nitrogen percentage are sufficiently high [16,33,34]. Instead, in the LN sample, only peaks of expanded austenite and Fe_4N are observed, whereas neither CrN nor Fe_3N were detected.

Fig. 5b and c shows a comparison of spectra obtained at 1 and 5° from HN and LN, respectively. They clearly show that in the 5° patterns, the contribution of all nitrides is lower than in the 1° spectrum and in LN, γ_N peaks are observed.

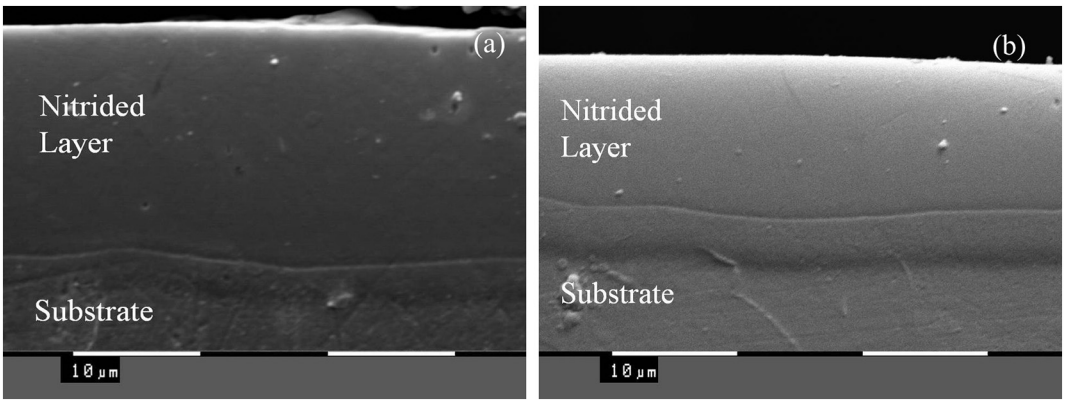

Fig. 1. Cross-section SEM micrograph of an AISI 316L treated by ion nitrided (a) HN and (b) LN.

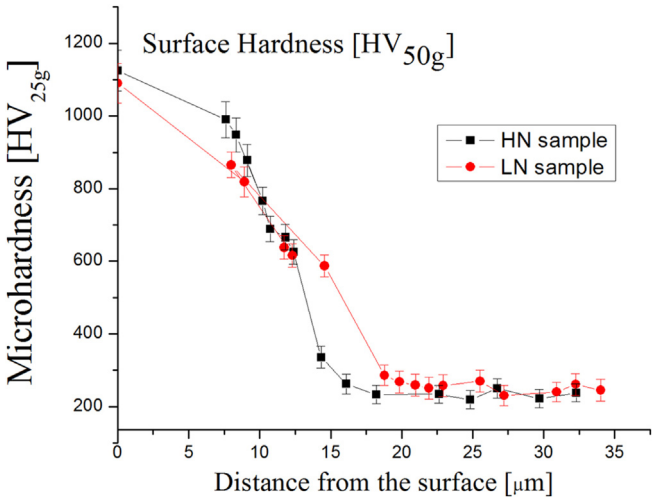

Fig. 3. Microhardness depth profiles of the nitrided HN and LN samples.

3.2. Corrosion tests

Fig. 6a displays the potentiodynamic polarization curves, showing the dependence of the current density *j* (in logarithmic scale) with the electrode potential *E* obtained in the environment of 3% NaCl solution for UN, HN and LN at room temperature.

The UN sample shows the typical behaviour of 316L, where the anodic branch of the curve presents the active-passive transition (pitting-passivation) followed by a passivation zone and finally by pitting corrosion and dissolution of the material. Localized corrosion, due to the action of chloride ions, starts at +0.30 V and manifests as spikes, which signals the onset of the pitting/repassivation process. Furthermore, the sharp increase in current at 0.37 V shows the evolution of pitting corrosion. Results of the three groups of samples are summarized in Table 5. HN and LN curves appear different. In the case of the HN, the corrosion potential is the most negative one, and the current does not show a true passive behaviour of the material at positive potentials, even though current increase is limited in some way, especially in the case of HN but current density is two decades higher than UN. The corrosion potential of LN is between UN and HN and the passive window is narrow. The current density of HN and LN is greater than the UN, although LN has a current density 30 times lower than HN at 2.5 V, the passive region of UN, and therefore a better performance against corrosion can be expected in this medium. The corrosion potential of HN is the most negative (least noble), followed by LN and UN.

Fig. 6b shows the potentiodynamic curves of UN, HN and LN in the Ringer's solution, and it was observed that the LN exhibits the noblest corrosion potential followed by UN and HN. The typical behaviour of pitting corrosion was observed for UN at +0.37 V and could not be clearly identified in the other samples. Regarding the current density, the HN had a current density greater than UN while in LN was lower throughout the test.

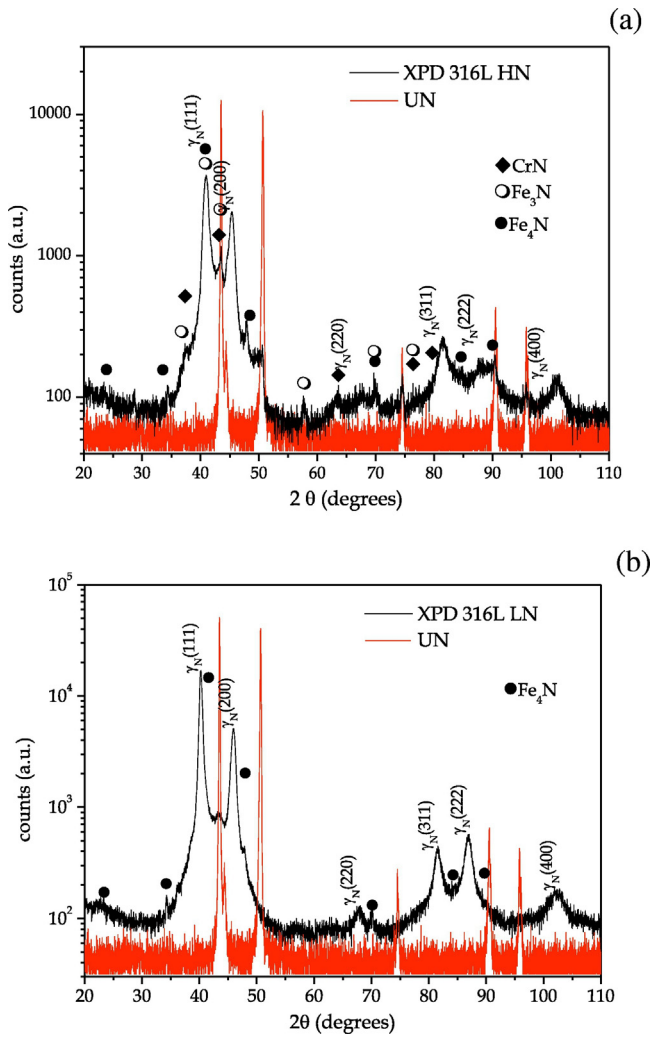

Fig. 4. X-ray spectra of (a) HN and (b) LN, both compared to the non nitrided sample (UN).

Table 3
Reflections corresponding to Fe nitrides and Cr nitrides in HN and LN.

2θ Fe_4N (HN and LN)	2θ $Fe_{2,3}N$ (HN)	2θ CrN (HN)
23.6°	38.1°	37.4°
33.7°	40.8°	43.5°
41.1°	43.3°	63.6°
48.0°	57.8°	76.3°
70.2°	68.8°	80.3°
84,8°	76.3°	–
89,5°	–	–

4. Discussion

SEM micrographs of Fig. 1 show that the nitrided layer appears clean in both nitriding conditions, continuous and uniform. In the optical micrograph it can also be seen free of dark areas associated with chromium nitride formation (Cr_xN) [35] and resistant to Marble reagent [36]. Also, as other authors discuss [29] the nitrided layer can be composed by an outer and an inner layer, with different N content and the inner layer is constituted by a γ_C carbon solid solution. Notably, at the end of nitrided layer, HN and LN, have shown a greater concentration of C than the average of the material. Carbon is contaminant coming from the reactor walls, and it is pushed back by N ions, this phenomenon is called "sweeping" [13,37,38].

Table 4
Penetration of X-rays at different angles.

Angle of incidence	X-ray penetration for different 2θ [nm]	
	30°	55°
1°	93	94
2.5°	219	228
5°	398	431
10°	634	768
Normal	713	1271

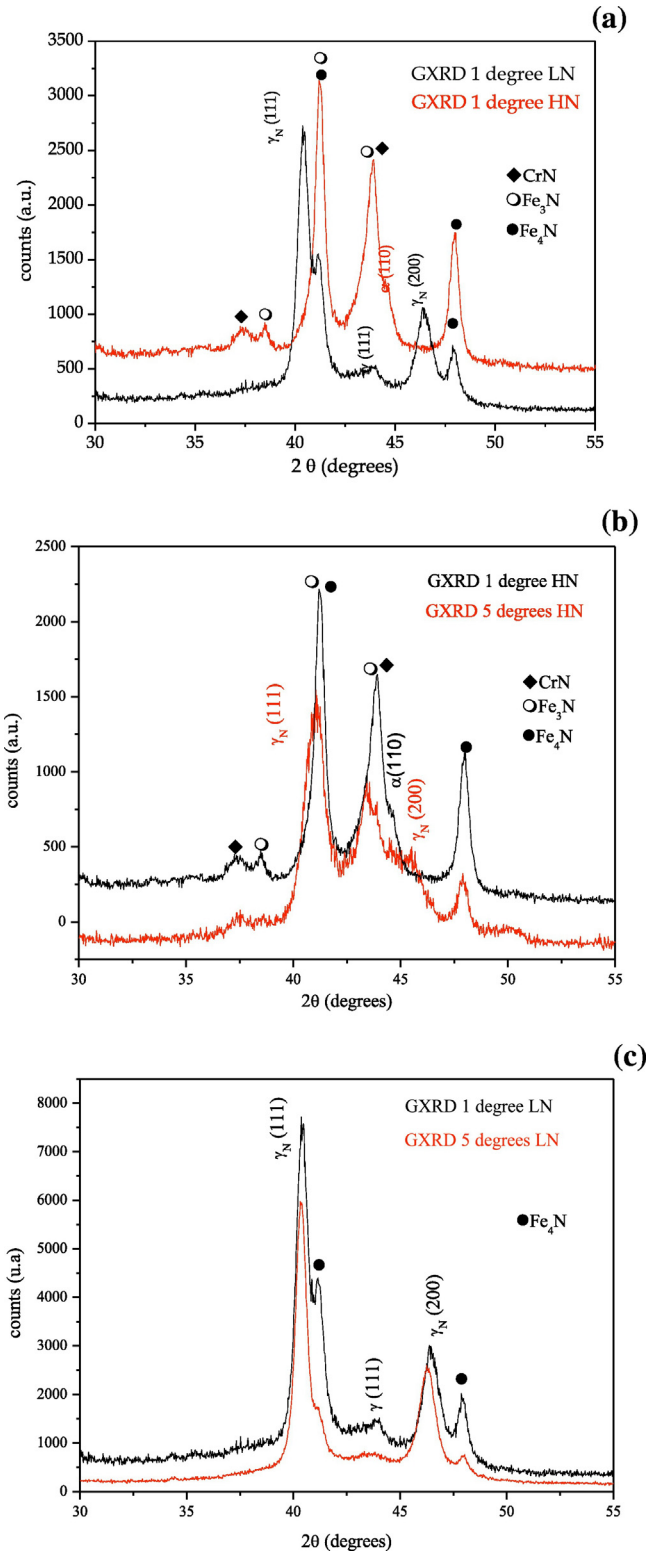

Fig. 5. X-ray patterns acquired with incidence of (a) 1°, comparing HN and LN. (b) and (c) 1 and 5° for each sample HN and LN respectively.

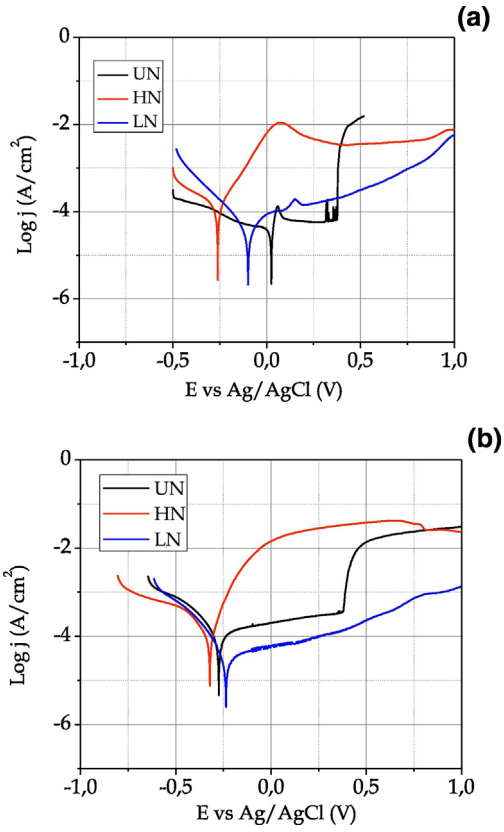

Fig. 6. Potentiodynamic curves of UN, HN and LN in (a) 3% NaCl solution and, (b) Ringer's solution.

This fact was proved with GDOES measurements presented in Fig. 2, showing the nitrogen depth profiles after ion plasma nitriding where N gradually decreases with depth, as reported by other authors [39]. However, this profile does not correspond to that obtained for the standard analytical equations of diffusion [39] which is due to sputtering effect that usually modifies N diffusion with respect to standard Arrhenius behaviour [39]. In fact, the thickness of the nitrided layer can be modified through the partial pressure of N in the treatment atmosphere as it was observed in this work and also previously [40,41]. The higher concentration of N led to an increased thickness of the nitrided layer, as was observed in HN compared to LN. Also, the high concentration of N observed in the area near to surface, could be due to the excess of N in the surface and some defects as such as dislocations, stacking faults, etc., product of the sputtering [1,39].

XRD analysis shows that the γ_N, detected on HN and LN samples, has peculiar features compared with γ of UN. Peaks of nitrided layer appear at lower Bragg angles than the peaks of UN. This effect may indicate expansion of the lattice owing to nitriding [17,42], presence of residual stresses, stacking faults [32] or porosity [1]. In addition to the shift in peaks position, the peaks are also broadened, which could be related to microstresses [1]. It should be noted here that there is no appreciable difference between HN and LN samples.

It is known that compressive residual stresses may contribute to higher surface hardness [1,30,43]. Also the surface hardness and microhardness profiles were similar between HN and LN, microhardness decreases gradually from the surface to base material (170 $HV_{0.05}$), profile with the same shape as N concentration profile in Fig. 2; therefore GIXRD was carried out.

Fig. 5a and b show the GIXRD diffraction of the HN and LN obtained by 1 and 5°. This provides a qualitative comparison of the phases present at different depths within the nitrided zone. In Fig. 2, it was observed that the nitrogen concentration decreases from the surface to the substrate, therefore it could be expected that the γ_N peaks to shift gradually to higher angles with increasing depth into the nitrided layer (1 and 5° by GIXRD) [44]. However, excess nitrogen in the surface leads to decomposition of the γ_N phase into α and iron and chromium nitrides [45]; effect that is mainly observed in HN resulting in a decrease in corrosion resistance. In LN the diffractogram shows Fe_4N and γ_N phase, but no Cr nitrides. These results indicate that the fractions of the CrN, Fe_3N and Fe_4N nitrides decrease continuously from the surface in HN and

Table 5
Quantitative results of corrosion tests in NaCl solution.

Samples	Epitting (V)	Ecorr (V)	J (A/cm^2) at −0.25 V
HN	–	~−0.3	4.7×10^{-3}
LN	–	~−0.1	1.5×10^{-4}
Untreated	~+0.40	~+0.05	6.3×10^{-5} (*)

(*) Passivation Current Density.

the same occurs in LN (except CrN). Fig. 2 demonstrates that the volume fraction of the nitrides at the surface layer decrease steadily with a decrease in the nitrogen percentage in the plasma nitriding atmosphere.

The potentiodynamic anodic polarization curves for the UN, HN and LN in 3% NaCl solution show that the corrosion current density for the UN sample is lower than the LN and HN samples, indicating that the UN is less reactive than LN and HN in the passivity potential range. HN and LN present corrosion potential shifted in the negative direction ($E_{corr} = -0.30$ V for HN). The corrosion current for HN and LN, respectively, are higher than UN, although corrosion current density of LN is lower than HN, and therefore present an improvement in corrosion resistance. Moreover, in the nitrided sample there was no abrupt current density increase as in the case of UN, just because there was no sign of crevice attack, as it can be seen in the micrographs showing that in the untreated sample, crevice corrosion was localized under the O-ring (Fig. 7). The nitrided layer is not passive but the current increase is limited by the pits small area. Clearly, the current density in both cases was kept far below the UN for high potentials. In the nitrided samples, small pits could be observed on the corrosion surface but not crevice, as it is shown in Fig. 8a and b.

Corrosion measurements demonstrate that the processing atmosphere during the plasma nitrided treatment has an important effect on the corrosion properties.

The plasma-nitriding improves the corrosion resistance when the S phase, a nitrogen supersaturated solution into the austenite phase, is formed. M.K. Lei et al. [46], among others [47], noted that a high concentration of nitrogen in nitrided layer (~32%) could delay pitting corrosion. The nitrogen in solution has an important role in improving electrochemical properties by forming ammonium ions which facilities the change of pH producing a local neutralizing effect at active sites. Moreover, nitrogen stabilizes the oxide film at the surface, preventing attack from chlorides anions [11,12]. However, as L. Gil et al. [48] reported for nitriding of stainless steels, our results for HN showed a negative effect on the corrosion resistance. This behaviour could be associated with the precipitation of CrN in the nitrided layer, which contributed to the depletion of chromium in the matrix. If the chromium content is below 11%, the steel is sensitized and when is exposed to an aggressive medium it is attacked [2,3,49,50]. In sample LN, CrN precipitation was avoided and the presence of Fe_4N did not deteriorate the corrosion resistance. This does not coincide with what is stated in the bibliography in which only phase S without nitrides presents good behaviour towards corrosion, if there is a mixed phase (nitrides and expanded austenite), the corrosion behaviour is similar to that of stainless steel [46]. But it does coincide to a certain extent with what some authors say

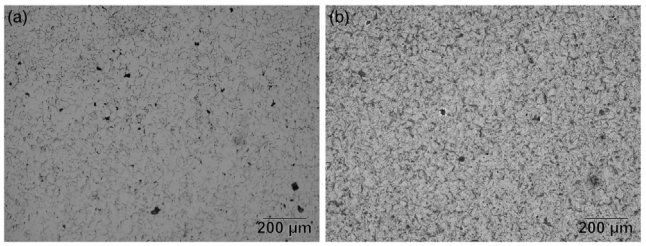

Fig. 8. Optical micrographs of the open tested surface in (a) HN sample, (b) LN sample. Small pits can be observed.

that there is a certain proportion of iron nitrides which can enhance resistance of nitrided steel [4].

The corrosion test in the Ringer's solution, Fig. 6b, shows that the LN curve is shifted at a more positive corrosion potential than UN. HN and LN curves indicate an active dissolution of the metal at more positive potentials than the corrosion potential. Even though, the LN sample exhibits a nobler corrosion potential than HN and UN, which also has the lowest current corrosion density among all samples.

Regarding the type of corrosion attack, crevice corrosion was observed in the untreated sample (Fig. 9). In the LN sample, no crevice was observed and only pitting corrosion could be detected (Fig. 10b); also grinding scratches can be seen before and after the corrosion test (Fig. 10a and b). However, the HN sample presented general corrosion combined with the formation of numerous pits as it can be observed in Fig. 11b, where the corrosion products covered all grinding scratches that could be seen before the test (Fig. 11a).

The LN sample had a certainly better corrosion resistance in Ringer solution than the untreated AISI 316L. In the literature, it is reported that the S-phase has the corrosion potential of stainless steel but it presents a pitting potential higher than stainless steel in Ringer's solution [51]. Some authors indicated that the high pitting potential of S-phase is related to its dissolving reaction ($[N] + 4H^+ + 3e \rightarrow NH_4^+$) for S-phase, it depends on the supersaturation of nitrogen in γ-phase and it can occur in Ringer's solution with pH from 3.5 to 7.2. The NH_4^+ ions have a local neutralizing effect in acidic pits on the corroded surfaces, increasing the pitting corrosion resistance in this solution [20]. This

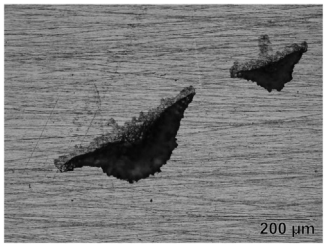

Fig. 9. Untreated sample surface under the O-ring after corrosion tests in Ringer's solution. Crevice corrosion could also be observed here.

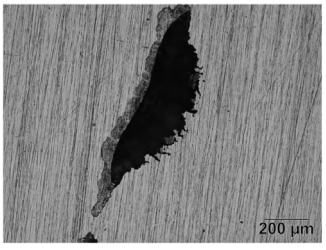

Fig. 7. Optical micrograph of untreated sample surface under the O-ring after corrosion tests in 3% NaCl solution.

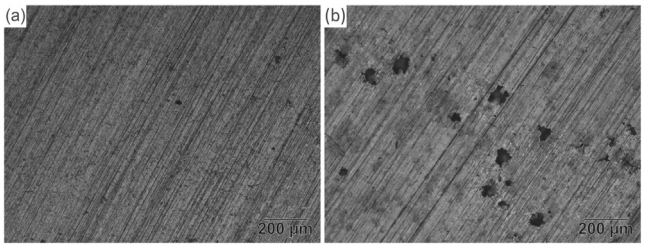

Fig. 10. (a) Open tested surface of the LN sample before corrosion tests in Ringer's solution (b) Open tested surface after corrosion tests in Ringer's solution.

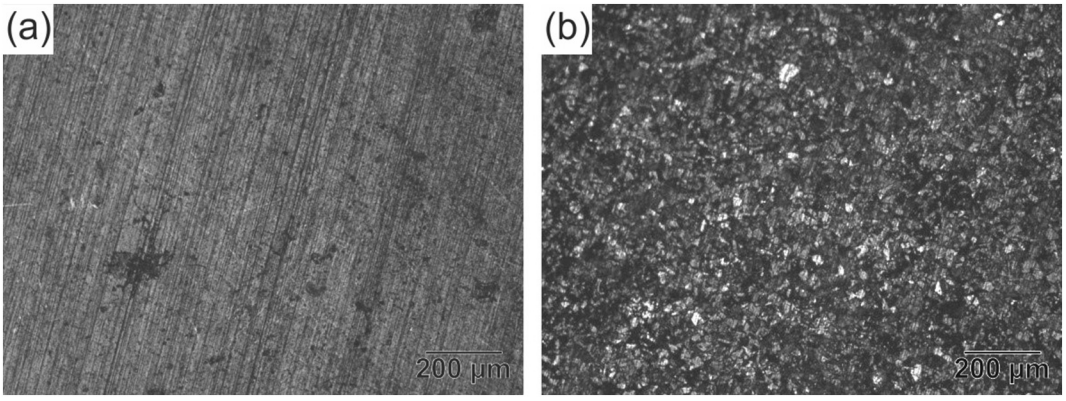

Fig. 11. (a) Open tested surface of the HN sample before corrosion tests in Ringer's solution (b) Open tested surface after corrosion tests in Ringer's solution.

reaction also can take place for other nitrogen-containing phases such as Fe_4N [20]. It is possible that in the LN sample, this reaction was favored due to the presence of S-phase and Fe_4N.

5. Conclusion

316L Samples were nitrided in two different N content atmospheres. The samples present a similar N concentration profiles, although HN shown a greater nitrogen content at all depths and a slightly higher penetration. However, microhardness profiles were similar to XRD diffraction. GIXRD diffraction confirmed the presence of CrN, Fe_3N and Fe_4N in HN samples and the absence of CrN in LN ones. This would explain that LN samples presented a better corrosion performance than HN samples, especially in Ringer's solution, where the nitrided samples with a lower nitrogen percentage presented a better behaviour than the base material.

This result is important regarding the use of DC ion nitrided steels for biomaterials, not only the temperature but also de nitrogen partial pressure is determinant to the microstructure and as a consequence to the corrosion resistance.

Acknowledgements

The authors are very grateful for the financial assistance granted by Instituto Nacional de Tecnología Industrial and PID Nº 00157/2000 (ANPCyT). The authors want to thank the collaboration received from Dr. Pablo Corengia Cabrera (Fundación INASMET-Tecnalia). We also gratefully acknowledge Belén Parodi and Leonardo Pazos from INTI for discussion and SEM micrograph.

References

[1] Y. Sun, X. Li, T. Bell, X-ray diffration characterization of low temperature plasma nitrided austenitic stainless steels, Mater. Sci. 234 (1999) 4793–4802.
[2] C.X. Li, T. Bell, Corrosion properties of active screen plasma nitrided 316 austenitic stainless steel, Corros. Sci. 46 (2004) 1527–1547.
[3] V. Singh, K. Marchev, C.V. Cooper, E.I. Meletis, Intensified plasma-assisted nitriding of AISI 316L stainless steel, Surf. Coat. Technol. 160 (2002) 249–258.
[4] S.D. de Souza, M. Olzon-Dionysioa, R.L.O. Basso, S. de Souza, Mössbauer spectroscopy study on the corrosion resistance of plasma nitrided ASTM F138 stainless steel in chloride solution, Mater. Charact. 61 (2010) 992–999.
[5] V.I. Dimitrov, J. D'Haan, G. Knuyt, C. Quasyhaegens, L.M. Stals, A method for determination of the effective diffusion coefficient and sputtering rate during plasma diffusion treatment, Surf. Coat. Technol. 99 (1998) 234–241.
[6] K. Marchev, M. Landis, R. Vallerio, C.V. Cooper, B.C. Giessen, The m phase layer on ion nitrided austenitic stainless steel (III): an epitaxial relationship between the m phase and the γ parent phase and a review of structural identifications of this phase, Surf. Coat. Technol. 116–119 (1999) 184–188.
[7] H. Kuwahara, H. Matsuoka, I. Tamura, J. Takada, S. Kikuchi, Y. Tomii, Effect of plasma on nitriding of Fe-18Cr-9Ni alloy, J. Mater. Sci. 27 (1992) 637–640.
[8] M.P. Fewell, D.R.G. Mitchell, J.M. Priest, K.T. Short, G.A. Collins, The nature of expanded austenite, Surf. Coat. Technol. 131 (2000) 300–306.
[9] K. Marchev, R. Hidalgo, M. Landis, R. Vallerio, C.V. Cooper, B.C. Giessen, The metaestable m phase layer on ion nitrided austenitic stainless steels part 2: crystal structure and observation of its two-directional orientational anisotropy, Surf. Coat. Technol. 112 (1999) 67–70.
[10] X. Xu, Z. Yu, L. Wang, J. Qiang, Z. Hei, Phase depth distribution characteristics of the plasma nitrided layer on AISI 304 stainless steel, Surf. Coat. Technol. 162 (2003) 242–247.
[11] A. Fossati, F. Borgioli, E. Galvanetto, T. Bacci, Corrosion resistance properties of glow-discharge nitrided AISI 316L austenitic stainless steel in NaCl solutions, Corros. Sci. 48 (2006) 1513–1527.
[12] A. Fossati, F. Borgioli, E. Galvanetto, T. Bacci, Glow-discharge nitriding of AISI 316L austenitic stainless steel: influence of treatment time, Surf. Coat. Technol. 200 (2006) 3511–3517.
[13] L.C. Gontijo, R. Machado, S.E. Kuri, L.C. Casteletti, P.A.P. Nascente, Corrosion resistance of the layers formed on the surface of plasma-nitrided AISI 304L steel, Thin Solid Films 515 (2006) 1093–1096.
[14] A. Alsaran, A. Çelik, C. Çelik, Determination of the optimum conditions for ion nitriding of AISI 5140 steel, Surf. Coat. Technol. 160 (2002) 219–226.
[15] G. Abrasonis, J.P. Rivière, C. Templier, S. Muzard, L. Pranevicius, Influence of surface preparation and ion flux on the nitriding efficiency of austenitic stainless steel, Surf. Coat. Technol. 196 (2005) 279–283.
[16] J. Wang, J. Xiong, Q. Peng, H. Fan, Y. Wang, G. Li, B. Shen, Effects of DC plasma nitriding parameters on microstructure and properties of 304L stainless steel, Mater. Charact. 60 (2009) 197–203.
[17] B.Y. Jeong, M.H. Kim, Effects of pulse frequency and temperature on the nitride layer and surface characteristics of plasma nitrided stainless steel, Surf. Coat. Technol. 137 (2001) 249–254.
[18] K.H. Lo, C.H. Shek, J.K.L. Lai, Recent developments in stainless steels, Mater. Sci. Eng. R 65 (2009) 39–104.
[19] J.A. Disegi, L. Eschbach, Stainless steel in bone surgery, Injury 31 (2000) D2–D6.
[20] M.K. Lei, X.M. Zhu, In vitro corrosion resistance of plasma source ion nitrided austenitic stainless steels, Biomaterials 22 (2001) 641–647.
[21] L.-H. Lin, S.-C. Chen, C.-Z. Wu, J.-M. Hung, K.-L. Ou, Microstructure and antibacterial properties of microwave plasma nitrided layers on biomedical stainless steels, Appl. Surf. Sci. 257 (2011) 7375–7380.
[22] C.F. Hung, C.Z. Wu, W.F. Lee, K.L. Ou, C.M. Liu, P.W. Peng, The effect of nitrided layer on antibacterial properties for biomedical stainless steel, Phys. Procedia 32 (2012) 914–919.
[23] K.-L. Ou, H.-H. Chou, C.-M. Liu, P.-W. Peng, Surface modification of austenitic stainless steel with plasma nitriding for biomedical applications, Surf. Coat. Technol. 206 (2011) 1142–1145.
[24] P. Corengia, G. Ybarra, C. Moina, A. Cabo, E. Broitman, Microstructural and topographical studies of DC-pulsed plasma nitrided AISI 4140 low-alloy steel, Surf. Coat. Technol. 200 (2005) 2391–2397.
[25] Y. Xia, S. Wang, F. Zhou, H. Wang, Y. Lin, T. Xu, Tribological properties of plasma nitrided stainless steel against SAE52100 steel under ionic liquid lubrication condition, Tribol. Int. 39 (2006) 635–640.
[26] B.D. Cullitty, Elements of X-Ray Difraction, Tercera ed. Addison-Wesley Publishing Company, Estados Unidos de América, 1956.
[27] S. Kumar, T.S.N. Sankara Narayanan, S. Ganesh Sundara Raman, S.K. Seshadri, Fretting corrosion behaviour of thermally oxidized CP-Ti in Ringer's solution, Corros. Sci. 52 (2010) 711–721.
[28] T. Moskalioviene, A. Galdikas, Stress induced and concentration dependent diffusion of nitrogen in plasma nitrided austenitic stainless steel, Vacuum 86 (2012) 1552–1557.
[29] T. Czerwiec, H. He, S. Weber, C. Dong, H. Michel, On the occurrence of dual diffusion layers during plasma-assisted nitriding of austenitic stainless steel, Surf. Coat. Technol. 200 (2006) 5289–5295.
[30] O.S.C. Blawert, H. Kalvelage, B.L. Mordike, G.A. Collins, K.T. Short, Y. Jiráskova, Nitrogen and carbon expanded austenite produced by PI3, Surf. Coat. Technol. 136 (2001) 181–187.
[31] Z. Cheng, C.X. Li, H. Dong, T. Bell, Low temperature plasma nitrocarburising of AISI 316 austenitic stainless steel, Surf. Coat. Technol. 191 (2005) 195–200.
[32] J.P. Riviere, M. Cahoreau, P. Meheust, Chemical bonding of nitrogen in low energy high flux implanted austenitic stainless steel, J. Appl. Phys. 91 (2002) 6361–6366.

[33] C. Alves Jr., J. de A. Rodrigues, A.E. Martinelli, Growth of nitrided layers on Fe–Cr alloys, Mater. Sci. Eng. A279 (2000) 10–15.
[34] G. Miyamoto, A. Yonemoto, Y. Tanaka, T. Furuhara, T. Maki, Microstructure in a plasma-nitrided Fe–18 mass% Cr alloy, Acta Mater. 54 (2006) 4771–4779.
[35] Y. Sun, T. Bell, Z. Kolosvary, J. Flis, The response of austenitic stainless steels to low-temperature plasma nitriding, Heat Treat. Met. 1 (1999) 9–16.
[36] C. Allen, C.X. Li, T. Bell, Y. Sun, The effect of fretting on the fatigue behaviour of plasma nitrided stainless steels, Wear 254 (2003) 1106–1112.
[37] M.J. Baldwin, S. Kumar, J.M. Priest, M.P. Fewell, K.E. Prince, K.T. Short, Plasma-nitrided AISI-316 stainless steel examined by scanning electron microscopy and secondary ion mass spectrometry, Thin Solid Films 345 (1999) 108–112.
[38] J.R.G. da Silva, R.B. McLellan, Diffusion of carbon and nitrogen in B.C.C. iron, Mater. Sci. Eng. 26 (1976) 83–87.
[39] T. Moskalioviene, A. Galdikas, J.P. Rivière, L. Pichon, Modeling of nitrogen penetration in polycrystalline AISI 316L austenitic stainless steel during plasma nitriding, Surf. Coat. Technol. 205 (2011) 3301–3306.
[40] E. Menthe, K.T. Rie, Further investigation of the structure and properties of austenitic stainless steel after plasma nitriding, Surf. Coat. Technol. 116–119 (1999) 199–204.
[41] E. Menthe, A. Bulak, J. Olfe, A. Zimmermann, K.-T. Rie, Improvement of the mechanical properties of austenitic stainless steel after plasma nitriding, Surf. Coat. Technol. 133–134 (2000) 259–263.
[42] N. Mingolo, A.P. Tschiptschin, C.E. Pinedo, On the formation of expanded austenite during plasma nitriding of an AISI 316L austenitic stainless steel, Surf. Coat. Technol. 201 (2006) 4215–4218.
[43] W. Liang, Surface modification of AISI 304 austenitic stainless steel by plasma nitriding, Appl. Surf. Sci. 211 (2003) 308–314.
[44] C. Templier, J.C. Stinville, P.O. Renault, G. Abrasonis, P. Villechaise, J.P. Rivière, M. Drouet, Nitrogen interstitial induced texture depth gradient in stainless steel, Scr. Mater. 63 (2010) 496–499.
[45] H. Dong, S-phase surface engineering of Fe-Cr, Co-Cr and Ni-Cr alloys, Int. Mater. Rev. 55 (2010) 65–98.
[46] M.K. Lei, X.M. Zhu, Plasma-based low-energy ion implantation of austenitic stainless steel for improvement in wear and corrosion resistance, Surf. Coat. Technol. 195 (2005) 22–28.
[47] J. Flis, J. Mankowski, T. Zakroczymski, T. Bell, S. Janosi, Z. Kolozsvary, B. Narowska, Surface films on plasma nitrided stainless steel subjected to passivation treatments, Corros. Sci. 41 (1999) 1257–1272.
[48] L. Gil, S. Brühl, L. Jiménez, O. Leon, R. Guevara, M.H. Staia, Corrosion performance of the plasma nitrided 316L stainless steel, Surf. Coat. Technol. 201 (2006) 4424–4429.
[49] N. Dingremont, E. Bergmann, M. Hans, P. Collignon, Comparison of the corrosion resistance of different steel grades nitrided, coated and duplex treated, Surf. Coat. Technol. 76-77 (1995) 218–224.
[50] M.K. Lei, Z.L. Zhang, Microstructure and corrosion resistance of plasma source ion nitrided austenitic stainless steel, J. Vac. Sci. Technol. A15 (1997) 421–427.
[51] E. Skolek-Stefaniszyn, J. Kaminski, J. Sobczak, T. Wierzchon, Modifying the properties of AISI 316L steel by glow discharge assisted low-temperature nitriding and oxynitriding, Vacuum 85 (2010) 164–169.